Monthly Notices
of the
ROYAL ASTRONOMICAL SOCIETY

Mon. Not. R. Astron. Soc. **403,** 1849–1858 (2010) doi:10.1111/j.1365-2966.2010.16254.x

Ionized gas outflow in the isolated S0 galaxy NGC 4460⋆

Alexei Moiseev,† Igor Karachentsev and Serafim Kaisin

Special Astrophysical Observatory, Russian Academy of Sciences, Nizhnii Arkhyz, Karachaevo-Cherkesskaya Republic, 369167 Russia

Accepted 2009 December 23. Received 2009 December 8; in original form 2009 October 1

ABSTRACT

We used integral-field and long-slit spectroscopy to study a bright extended nebulosity recently discovered in the isolated lenticular galaxy NGC 4460 during an Hα survey of nearby galaxies. An analysis of archival Sloan Digital Sky Survey, *GALEX* and *Hubble Space Telescope* images indicates that current star formation is entirely concentrated in the central kiloparsec of the galaxy disc. The observed ionized gas parameters (morphology, kinematics and ionization state) can be explained by a gas outflow above the plane of the galaxy, caused by star formation in the circumnuclear region. Galactic wind parameters in NGC 4460 (outflow velocity, total kinetic energy) are several times smaller, compared with the known galactic wind in NGC 253, which is explained by the substantially lower total star formation rate. We discuss the cause of the star formation processes in NGC 4460 and in two other known isolated lenticular (S0) and elliptical (E) galaxies of the Local Volume: NGC 404 and 855. We provide evidence suggesting that the feeding of isolated galaxies by intergalactic gas on a cosmological time-scale is a steady process without significant variations.

Key words: galaxies: elliptical and lenticular, cD – galaxies: individual: NGC 4460 – galaxies: ISM – galaxies: kinematics and dynamics – galaxies: starburst.

1 INTRODUCTION

Isolated elliptical (E) and lenticular (S0) galaxies are rare objects, whose properties differ appreciably from E and S0 galaxies in clusters and groups. Among the 513 most isolated galaxies of the Local Universe with radial velocities $V_{\rm LG} < 3500$, only 19 systems (i.e. about 4 per cent) belong to types E and S0 (Karachentsev et al. 2010). Isolated E and S0 galaxies are characterized by low luminosity ($M_B \simeq -17.6$ mag), bluer-than-average colours and the appreciable presence of gas and dust. The nearby S0 galaxy, NGC 404, with $M_B = -16.6$ mag, is a typical example; it has been found to host an extended H I shell (Del Rio, Brinks & Cepa 2004) and an ultraviolet (UV) bright ring of young stars (Thilker 2009). Among ∼450 Local Volume (LV) galaxies with heliocentric distances $D < 10$ Mpc (Karachentsev et al. 2004), there are only three E and S0 galaxies with absolute magnitudes ($-16.0 > M_B > -18.0$) and negative 'tidal indices' $TI < 0$; these galaxies (NGC 404, 855 and 4460) have therefore been classified as isolated objects. These objects seem to be local analogues of 'blue-sequence E/S0' galaxies, recently identified by Kannappan, Guie & Baker (2009), which might form a transition population between late-type spirals/iregulars and early-type red-sequence galaxies.

An extensive Hα survey of LV galaxies has been carried out in recent years with the 6-m telescope of the Special Astrophysical Observatory of the Russian Academy of Sciences (SAO RAS) in order to determine the rates of star formation in a representative distance-limited sample of galaxies. An analysis of the population of Canes Venatici I scattered cloud of nearby galaxies has revealed (Kaisin & Karachentsev 2008) that the circumnuclear region in NGC 4460 hosts bright Hα line emission (see Fig. 1), which must be indicative of ongoing star formation. Such a phenomenon appears to be non-typical in an isolated early-type galaxy. This bright emission may be the result of a recent merger of NGC 4460 with a gas-rich companion, or of the impact of a massive intergalactic H I cloud on to the central region of NGC 4460. In this case, the Hα nebulosity, which extends along the major axis of the galaxy, may be the product of a recent interaction. An analysis of the kinematics and ionization state of the gas in NGC 4460 helps us understand the nature of this mysterious phenomenon. With this aim, we have analysed the available archival images of the galaxy and performed spectroscopic observations of NGC 4460 with the SAO RAS 6-m telescope. Following Tonry et al. (2001), we adopt the distance to the galaxy of 9.59 Mpc, which corresponds to a scale of 46.5 pc arcsec^{-1}.

⋆Based on observations collected with the 6-m telescope of the Special Astrophysical Observatory of the Russian Academy of Sciences, which is operated under the financial support of the Science Department of Russia (registration number 01-43).
†E-mail: moisav@gmail.com

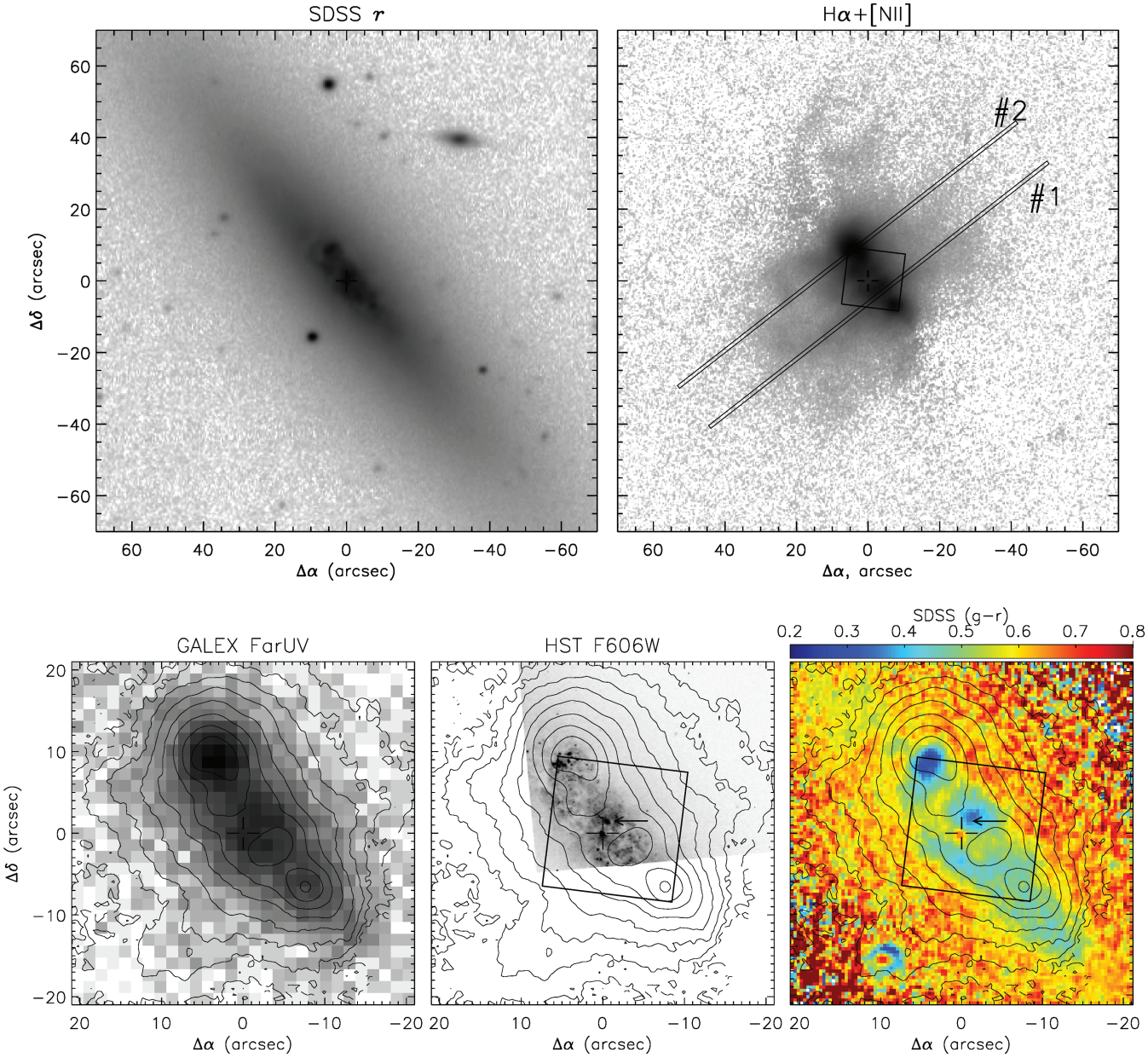

Figure 1. Images of NGC 4460 in logarithmic brightness scale. The upper row shows the SDSS *r*-band image (left) and the Hα + [N II] image (right) taken with the 6-m telescope (Kaisin & Karachentsev 2008). The locations of the spectrograph slits are shown. Hereafter, the black square marks the MPFS field of view. The lower row contains the images of the centre of the galaxy with Hα line contours superimposed based on the *GALEX* far-UV data (left), the *HST* WFPC/606W optical map (centre) and the map of the (g–r) colour index according to the SDSS (right). The cross marks the galaxy nucleus that coincides with the kinematic centre derived from MPFS data. The arrow shows the position of the second circumnuclear knot (see text).

2 PHOTOMETRIC STRUCTURE OF THE GALAXY

2.1 Circumnuclear region

A comparison of the Hα+[N II] image of the galaxy with broadband Sloan Digital Sky Survey (SDSS) images (Fig. 1) convincingly demonstrates that most of the emission-line radiation emerges from a compact region in the disc inside the radius $r < 20$ arcsec. This is where all H II regions are located, whereas diffuse Hα+[N II] emission extends along the minor axis of the galaxy on both sides of its nucleus. An analysis of optical and UV images shows that ongoing star formation in NGC 4460 is concentrated entirely inside the central kiloparsec. This follows from the distribution of far-UV radiation (λ1344–1786 Å) according to *GALEX* archival data, and is exactly coincident with the circumnuclear H II regions (Fig. 1). Also, the young stellar population found in this region stands out because of its bluer colour index in the SDSS images (see Fig. 1). Star-forming regions make an almost closed ring in the disc of the galaxy. The *r*-band image reveals a compact nucleus with $(g–r) = 0.65$, whereas a condensation located 1.5–2 arcsec north of the nucleus (marked with an arrow in Fig. 1) becomes brighter in blue filters with the colour $(g–r) = 0.45$. On the *Hubble Space Telescope* (*HST*) optical image, this circumnuclear knot corresponds to a compact stellar cluster with a linear size FWHM = 17 × 10 pc, whose luminosity is only twice as low as that of the compact cluster in

the 'main' nucleus. We note that the dynamical centre of the gas velocity field (marked with crosses in Figs 1 and 3) coincides with the main nucleus of the galaxy (see Section 5). The circumnuclear star-forming regions have evidently different evolutionary status, because only north-east of the nucleus does the peak of Hα emission coincide with the 'blue' region on the (g–r) map. At the same time, the two blue regions near the minor axis (including the second nucleus) are not associated with Hα+[N II] peaks. These regions must have already lost most of their gas or lack OB stars needed for its ionization.

The SDSS images exhibit individual dust lanes in the inner part of the region. On the *HST* image, these lanes can be easily seen to border H II regions, and they are most probably associated with dense gas compressed by shocks produced by star-forming processes (supernova explosions and winds from massive stars).

2.2 Orientation of the disc and the brightness distribution

Using isophotal analysis of SDSS images, we found the position angle and ellipticity of the outer r- and i-band isophotes to be PA $= 39\overset{\circ}{.}5 \pm 0\overset{\circ}{.}4$ and $\epsilon = 0.71 \pm 0.02$. According to the empirical relation (Hubble 1926), this implies a galaxy inclination of $i = 77^\circ \pm 1^\circ$. We used the inferred orientation parameters to construct the azimuthally averaged surface-brightness profiles of *ubvri* SDSS images. In all filters, the brightness distribution is almost exactly exponential at $r > 30$–40 arcsec, with the brightness excess at $r <$ 20 arcsec being more conspicuous in blue filters; this represents star-forming regions. Fig. 2 shows the decomposition of the r-band surface brightness profile into components. After the subtraction of the outer disc ($\mu_0 = 19.4$ mag, $h = 29.5$ arcsec), the brightness excess still remains at $r < 30$–40 arcsec. However, it is not a bulge, because after the subtraction of the two-dimensional disc model the brightness contours of the residual image have the same ellipticity as those of the outer disc. The brightness profile at the centre can be described well by a second exponential function with almost the same central brightness ($\mu_0 = 19.2$ mag), but with a three times shorter scalelength, $h = 11.5$ arcsec. At the centre, we can see a low-contrast compact nucleus as described above.

Thus, it follows that only some of the morphological features (smooth outer isophotes, lack of spiral arms) suggest that NGC 4460 may be a lenticular galaxy. However, the bulge/disc ratio is indicative of a later morphological type, because the spherical component is barely visible in the brightness distribution. Inner exponential discs are often referred to as 'pseudo-bulges' (Kormendy & Kennicutt 2004). However, the corresponding feature in NGC 4460 is indeed a bona fide disc whose thickness, according to photometric data, coincides with that of the outer disc.

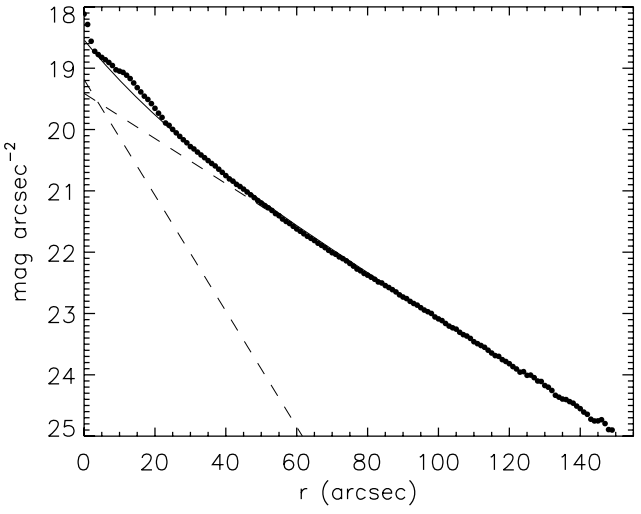

Figure 2. Decomposition of the r-band surface brightness profile (dots) into two discs (dashed line). The solid line marks the sum of both disc models.

Multitiered (antitruncation, according to the classification by Erwin, Beckman & Pohlen 2005) discs have been found increasingly often in spiral and lenticular galaxies. These are attributed either to slow internal secular evolution, which can only develop in the presence of a bar and/or a spiral (see Kormendy & Kennicutt 2004, for a review), or to a recent minor merging event. Both cases imply the loss of angular momentum, caused by some of the gas moving towards the centre, where a burst of star formation currently occurs, and the newly born stars form the inner disc with a short scalelength. There is also evidence of the recent formation of the inner disc because its contribution to the combined brightness profile (Fig. 2) is almost everywhere smaller than that of the main disc of the galaxy.

2.3 Bar or ring?

In Section 2.1, we mentioned that the star-forming regions make an almost closed ring in the central kpc. At first sight, the observed distribution of the H II regions has another interpretation, where the two brightest condensations, located almost equidistant from the nucleus $\sim$10 arcsec to the north-east and south-west, belong to the ends of a stellar bar. In this case, the two blue regions appearing on the colour-index map (Fig. 1) at $r = 2$–4 arcsec (including the off-nuclear compact cluster mentioned above) can be considered as part of the nuclear compact ring formed on the resonances of this bar.

However, this assumption contradicts other morphological features. First, there is a significant asymmetry in the properties of the two brightest H II regions. These have different sizes, Hα luminosities and colour indices (i.e. they have a different history of formation). This is strange in the case of lobes on the ends of a bar, which should be formed simultaneously. Secondly, the dust in the circumnuclear region has a chaotic distribution (Section 2.1) instead of the sharp curved dust lanes expected in a bar. Finally, the isophotal analysis of SDSS red images does not support any significant changes of ellipticity and PA of isophotes at the distances corresponding to the possible bar.

The effect of non-circular gas motions (radial inflow) could also be insufficient in the observed gas velocity field, because the major axis of the possible bar coincides with the galaxy line of nodes. Therefore, the regular velocity pattern in the circumnuclear region of the ionized gas velocity field (Section 5) cannot be used as an argument for or against the bar. We believe that only data on stellar kinematics can provide evidence for the existence (or absence) of a stellar bar in NGC 4460. However, our analysis of galactic photometry presented above suggests that the star-forming pseudo-ring, 2 kpc in diameter, nested in the inner stellar disc, is a more reliable description of the observed morphology.

3 OBSERVATIONS AND DATA REDUCTION

Long-slit and integral-field (three-dimensional) spectral observations were made at the prime focus of the SAO RAS 6-m telescope. The 2048 $\times$ 2048 EEV 42–40 CCD was used as a detector in both cases.

The central region of NGC 4460 was observed with the Multi-Pupil Fibre Spectrograph (MPFS). The MPFS (Afanasiev, Dodonov

Table 1. Log of spectral observations.

Date	Device	Position	T_{exp} (s)	Spectral range (Å)	Spectral resolution (Å)	Seeing (arcsec)
2007 Mar 27/28	MPFS	Nucleus	1800	5800–7300	3.5	1.7
2007 May 15/16	SCORPIO/LS	PA =128°, offset 5 arcsec to SW	1200	6050–7100	2.5	1.7
2007 May 15/16	SCORPIO/LS	PA =128°, offset 9 arcsec to NE	900	6050–7100	2.5	1.8

& Moiseev 2001) takes simultaneous spectra from 256 spatial elements (constructed in the shape of square lenses), which form on the sky an array of 16 × 16 elements ('spaxels') with the angular size 1 arcsec spaxel^{-1}. A bundle of 17 fibres placed at a distance about 3.5 arcmin from the lens array provides the night-sky background spectra simultaneously with object exposition. The spectral range included bright emission lines of ionized gas: Hα, [N II]$\lambda\lambda$6548, 6583 and [S II]$\lambda\lambda$6717, 6731. Fig. 1 shows the locations of the MPFS lens array on the galaxy image; the log of observations is presented in Table 1. The spectra were reduced using IDL-based software; the data reduction sequence is briefly described in Moiseev, Valdés & Chavushyan (2004). The data reduction results in a data cube in which a spectrum corresponds to each image 'spaxel' in a two-dimensional field 16 × 16 arcsec^2. The data cube was flux-calibrated using standard star observations taken on the same night, just after observations of the galaxy. The maps and velocity fields of the Hα, [N II] and [S II] emission lines were constructed using a single-Gaussian fitting.

The long-slit observations have been made with the multimode focal reducer SCORPIO (Afanasiev & Moiseev 2005). We obtained two cross-sections in a direction near-perpendicular to the galactic major axis, along extended Hα filaments and through bright H II regions in the galaxy disc (hereafter slits 1 and 2; see Fig. 1). The slit width was 1 arcsec and the scale along the slit was 0.35 arcsec px^{-1}; the log of observations is given in Table 1. The slit spectra were reduced and calibrated using the IDL-based software, developed at the SAO RAS. The parameters of the emission lines (FWHM, flux, velocity) were calculated from a single-Gaussian fitting. A multicomponent structure of the emission-line profiles was not detected as well as in the MPFS spectra. The long-slit spectra are deeper, because the SCORPIO quantum efficiency is significantly higher than that of the MPFS. This allows us to detect the weak emission lines [O I]$\lambda\lambda$6300, 6360 and He Iλ6678 in the brighter H II regions in the galactic disc.

4 PARAMETERS OF IONIZED GAS

Fig. 3 shows several maps based on MPFS data. The Hα brightness distribution agrees well with the narrow-band filter image discussed above. The continuum image exhibits a central condensation extending along the north–south direction. Given the lower spatial resolution of the MPFS compared to the SDSS data, the condensation must correspond to the double nucleus described in Section 2.1. The MPFS field of view contains three bright H II regions. The maps of the [N II]/Hα and [S II]/Hα flux ratios indicate a slight enhancement of forbidden-line emission around the star-forming regions,[1] whereas the corresponding ratios are minimal at the centres of the H I regions (see Fig. 3). In the space between star-forming regions,

[1] Hereafter, we use [N II]/Hα and [S II]/Hα ratios to denote the [N II]λ6583/Hα and [S II](λ6717 + λ6731)/Hα line flux ratios, respectively.

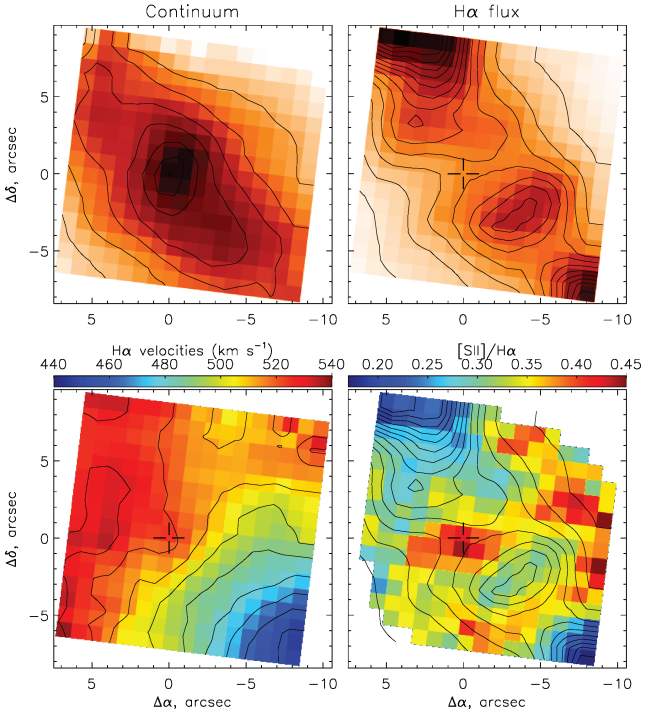

Figure 3. Results of MPFS observations. The top row shows the continuum image taken near λ6400 Å (left) and the Hα map (right). The bottom row shows the Hα velocity field (left) and the map of the [S II](λ6717 + λ6731)/Hα flux ratio with Hα contours superimposed (right). The coordinate origin coincides with the dynamic centre (cross).

we most likely observe hot gas ejected from these regions and ionized, among other factors, by shocks. The presence of shock fronts around the H II regions is further evidenced by dust lines seen at these locations (Section 2.1). In these places, the [S II]/Hα ratio reaches 0.45, which is close to the usually adopted border between shock ionization and photoionization (see below).

Fig. 4 shows variations of the emission-line parameters (flux, radial velocity, FWHM corrected for instrumental broadening) along the slits. The maximum of the emission-line brightness is therefore shifted relative to the peak in brightness of the stellar continuum, because bright H II regions in the circumnuclear ring do not lie on the major axis of the galaxy. Beyond the disc, surface brightness in the nebulosity decreases almost exponentially and emission lines can be detected at an even greater distance from the disc than on the Hα+[N II] image. The [S II]/Hα intensity ratio increases with increasing distance from the H II regions, whereas the corresponding increase of the [N II]/Hα ratio is less evident (see Fig. 4).

To identify the source of gas ionization, we constructed a diagnostic diagram showing the ratios of the fluxes of lines with different excitation mechanisms and similar wavelengths so that the result would not depend on dust extinction. Unfortunately, we

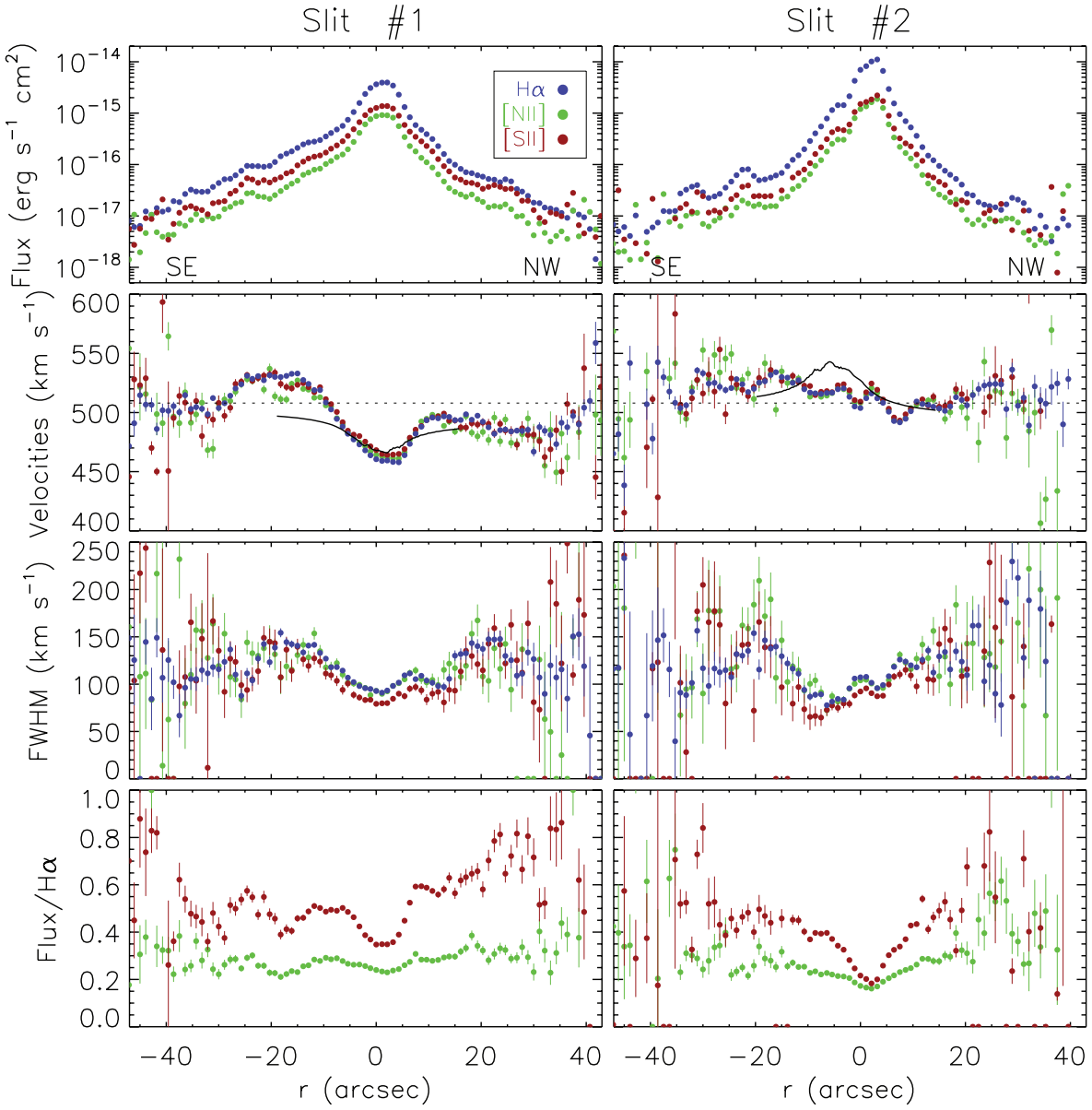

Figure 4. Measurements of the parameters of Hα, [N II]λ6583 and [S II]λ6717 + 6731 emission lines along slits 1 (left) and 2 (right). From top to bottom, we show the surface brightness, the line-of-sight velocity, the FWHM (corrected for the widths of the instrumental profile) and the line-to-Hα flux ratio. The dashed and solid lines show the systemic velocity (according to MPFS data) and the cross-section of the model velocity field, respectively.

can construct only one such diagram in the wavelength interval considered: [N II]/Hα versus [S II]/Hα (Fig. 5). The dashed lines separate regions with different excitation mechanisms, indicated as 'photoionization' and 'shock'. We assume, in accordance with Stasińska et al. (2006), that in the case of ionization by young stars the line ratios follow the relations: $\log[\mathrm{S\,II}]/\mathrm{H}\alpha < -0.4$ and $\log[\mathrm{N\,II}]/\mathrm{H}\alpha < -0.4$. A higher relative intensity of forbidden lines means that shocks, or even a non-thermal source (active galactic nucleus), contribute appreciably to ionization. When interpreting the positions of data points on the diagram, we must bear in mind the following: (i) the boundaries of the photoionization domain are controversial (i.e. the boundaries are determined not only by particular models, but also by the statistics of observations of different galaxies samples); (ii) in real objects, the combined effect of several ionization sources is present. Thus, according to Stasińska et al. (2006), the $-0.2 < \log[\mathrm{N\,II}]/\mathrm{H}\alpha < -0.4$ domain corresponds to a composite source of ionization in low-ionization nuclear emission-line region (LINER) type galaxies: photoionization by stars plus the effect of shocks, and shocks dominate only at $\log[\mathrm{N\,II}]/\mathrm{H}\alpha > -0.4$. Note that many researchers use an even more strict criterion (e.g. $\log[\mathrm{N\,II}]/\mathrm{H}\alpha > 0$ in Veilleux, Cecil & Bland-Hawthorn 2005).

Fig. 5 shows that the gas in the circumnuclear region (i.e. the central part observed with the MPFS, and the $r < 5$ arcsec regions in slit 1 and $r < 10$ arcsec regions in slit 2) is ionized by young stars. In the outer filaments, shock ionization begins to dominate with increasing distance from the disc plane, according to the [S II]/Hα criterion. At the same time, the [N II]/Hα criterion indicates that all our measurements, except several data points with $r \approx 30$ arcsec in slit 2, lie in the photoionization domain. However, in this case we consider the latter criterion to be less important, because the observed line ratio agrees well with the results of model

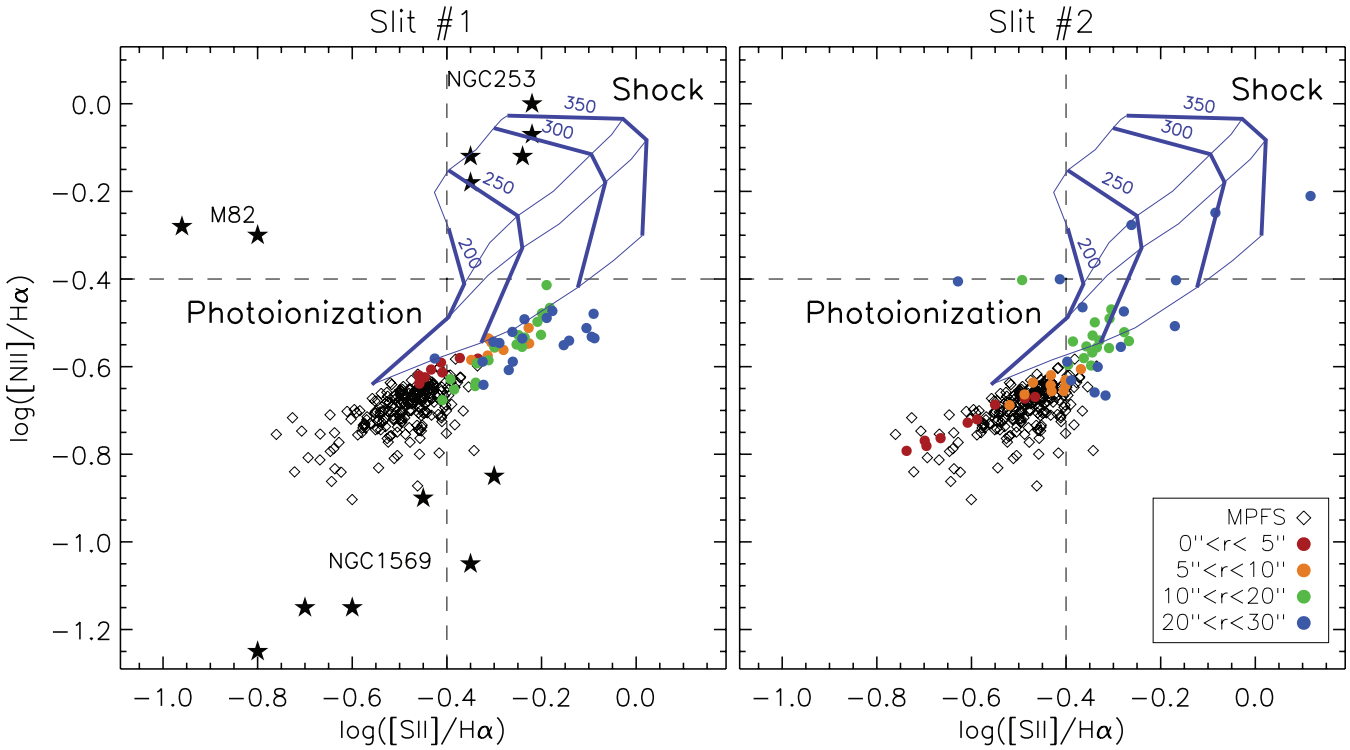

Figure 5. Diagram of the [N II]/Hα versus [S II]/Hα flux ratios. The dashed line separates domains with different ionization mechanisms. The blue lines show the grid of shock + precursor ionization models according to Allen et al. (2008) for $n = 1$ cm^{-3} and solar elemental abundances. The thin and bold blue lines mark the contours of the constant magnetic parameter 0.001, 0.5, 1 and 5 μG cm$^{2/3}$ (from bottom to top) and the contours of constant shock velocity (labelled in km s^{-1}), respectively. The circles show the measurements made along slits 1 (left) and 2 (right). Different colours correspond to different distances along the slits. The diamond symbols indicate the results of MPFS measurements for the circumnuclear region. The star symbols in the left-hand figure show the measurements for the regions of galactic wind in M82 (Westmoquette et al. 2009), NGC 253 (Matsubayashi et al. 2009) and NGC 1569 (Heckman et al. 1995).

computations (Allen et al. 2008) for shock + precursor ionization with number density $n = 1$ cm^{-3} and solar metallicity. Fig. 5 shows the grid of parameters for this model. It is evident from this figure that with increasing r the observed data points lie along the lines of increasing shock velocity from 200 to 300 km s^{-1} for small values of magnetic parameter 0–1 μG cm$^{2/3}$. For the estimation of gas metallicity, we used the data of slit 2, which passes through the centre of the brightest H II region, where the [N II]/Hα ratio is minimal and equal to 0.16 ± 0.03. If we assume that the shock contribution is minimal at this location, then the approximation of Stasińska et al. (2006) implies a gas metallicity of 0.74 ± 0.04 Z$_\odot$ (i.e. the solar-metallicity approximation is applicable to NGC 4460).

Thus, it follows that gas ionization in the extended Hα nebulosity can be explained by the combined effect of shocks and photoionization by young stars, with the latter dominating in the inner regions. The galaxy lacks an active nucleus, and therefore the likely cause of shocks is star formation. Gas is blown above the plane of the galaxy by the combined action of supernovae and stellar winds from young massive stars. This phenomenon is known as a 'galactic wind' (see a review by Veilleux et al. 2005). For comparison, we present in Fig. 5 the line ratios for three well-studied galaxies, where the existence of galactic wind has long been proven: M82, NGC 253 and 1569. For M82, we give two average values obtained by Westmoquette et al. (2009), who have used DensePak and GMOS instruments. We adopt the galactic-wind data for NGC 253 from fig. 5 in Matsubayashi et al. (2009), and for NGC 1569 we give several estimates for external emission regions adopted from fig. 7 in Heckman et al. (1995), for slit PA =70° and $r = \pm 20$, ± 50 and ± 70 arcsec from the centre. On the diagnostic diagram, the published data for these well-known galactic winds are scattered in a relatively wide range (± 0.5 dex), which also includes the data points for NCC 4460. Shock contribution to gas ionization in the filaments of NCC 4460 is comparable to galactic winds for all three galaxies previously studied. Moreover, the [S II]/Hα ratio in NGC 4460 is comparable with the values observed in NGC 253 and 1569. This is not for [N II]/Hα, because the intensity of the nitrogen doublet also depends on metallicity. For instance, the [N II]/Hα ratio in NGC 253 is most likely a result of the nitrogen overenrichment of the interstellar medium (Matsubayashi et al. 2009).

We use the [S II] line doublet ratio to estimate the electron density n_e in accordance with the relation of Osterbrock (1989) for $T_e = 10\,000$ K. Fig. 6 shows the radial variations of the line ratio and the corresponding values of n_e. Unfortunately, the relation of Osterbrock can be applied with confidence only at $n_e > 50$–100 cm^{-3}, whereas at low densities the slope of the ([S II]λ6717/λ6731 versus n_e) relation flattens and therefore leads to large uncertainties. Although the observed line ratio lies mainly inside this 'inconvenient' interval, it is safe to conclude that the density of emitting gas is lower than 100 cm^{-3} in the disc of the galaxy. The outer filaments exhibit a large scatter of density values ranging from zero to 200–300 cm^{-3}. It might be supposed that in the outer regions the spectrograph slit crosses individual clumps with ahighly non-uniform density distribution.

5 GAS KINEMATICS

The Hα-line velocity field, based on MPFS measurements (Fig. 3), can be described well in terms of the model of circular rotation of

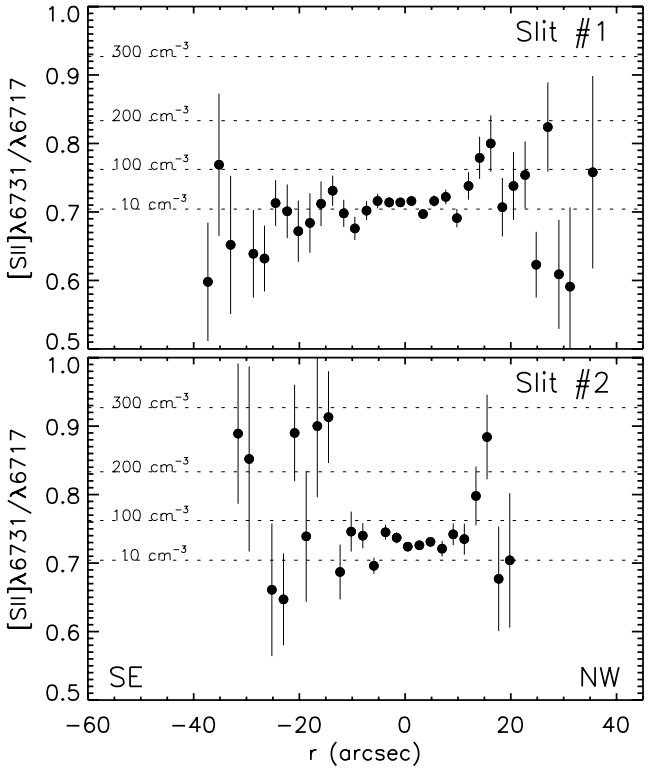

Figure 6. Variation of the [S II] line doublet ratio for slit 1 (top) and slit 2 (bottom). The horizontal dashed lines indicate the values of the corresponding electron density, which are labelled on the left.

the thin disc. The line-of-sight velocities measured by the [N II] and [S II] lines show no appreciable deviations from the Hα line-of-sight velocities. The centre of rotation, defined as the symmetry centre of the velocity field, coincides with the centre of the continuum image.

We constructed the model of rotation using the method described by Moiseev et al. (2004) with the position angle and inclination of the disc fixed in accordance with photometric data (Section 2.2). The PA measured from the velocity field agrees with the photometric position angle within the errors. The systemic velocity is $V_{\rm sys} = 508 \pm 5$ km s^{-1}. The rotation curve shows solid-rotation increase up to $v_{\rm max} = 67$ km s^{-1} at $r = 20$ arcsec, which is the border of the MPFS field of view. This value is close to the maximum rotation velocity according to H I measurements (Sage & Welch 2006). Observed velocities deviate from the corresponding model values by up to 20 km s^{-1} along the minor axis of the galaxy. This behaviour is most probably indicative of gas ejection above the plane of the galaxy. It could also be a result of uncertainties in the model: the thin-disc approximation may perform poorly at $i = 77^\circ$, internal absorption should be taken into account, etc.

The ionized gas velocity field in the compact star cluster region, noted on optical images ∼2 arcsec north of the nucleus (see Section 2.1), does not show any kinematic peculiarities, such as non-circular motions or a shift of the rotation centre. Therefore, our data do not support that this cluster is a nucleus of a dwarf satellite – a merging remnant. New high-resolution stellar kinematics data are needed in order to understand the origin of this offset cluster.

To estimate the peculiar velocities of the outer filaments, we extrapolate our model out to greater distances, assuming that the rotation curve reaches a plateau. Fig. 4 compares the model extrapolation and observed velocities in slit cross-sections. Slit 1 shows good agreement between the model and observations at $r < 15$ arcsec in the north-west half of the nebulosity. However, its more extended south-east half exhibits appreciable deviations already beyond 7–10 arcsec from the centre with the discrepancies amounting to 30–35 km s^{-1}. Slit 2 passes farther from the centre, along the edge of the field of view of the MPFS. Therefore, here deviations from the model extrapolation are more conspicuous in the disc region. On the whole, we may conclude that in the outer filaments systematic deviations of the observed line-of-sight velocities from the corresponding model values do not exceed, on average, 30 km s^{-1}. This implies an outflow velocity of $v_{\rm out} \approx 130$ km s^{-1}, if we assume that the observed peculiar gas motions are directed perpendicularly to the plane of the disc and if we take the projection effect into account. This value is comparable to the observed half-width of emission lines, which amounts to 150–170 km s^{-1} at a distance of $r = 20$–30 arcsec (0.9–1.4 kpc), whereas the FWHM is half in the disc. The fact that the amplitudes of regular velocities are approximately equal to those of chaotic velocities is indicative of strong turbulence in the filament gas.

6 DISCUSSION

6.1 Galactic wind

We have shown above that the peculiarities of the distribution of the parameters of ionized gas (kinematics, density and the state of ionization) observed in NGC 4460 can be most easily explained in terms of the 'galactic wind' hypothesis (i.e. assuming that the gas outflow above the plane of the galaxy is produced by a central burst of star formation). The alternative assumption, suggesting that we are observing remnants of a tidally disrupted gas-rich companion, is ruled out, because this would imply that line-of-sight velocities in the filaments should deviate significantly from the systemic velocity. Besides the above indicators, the shape of the emission nebulosity also suggests the presence of galactic wind. The nebulosity resembles a butterfly or, rather, two bubbles expanding above the plane of the galaxy. Note that the diameter of the bubble has become greater than the half-width of the gaseous disc; it has an open vertex, because the top of the bubble is no longer compressed by the ambient gas. Moreover, the emission nebulosity resembles the well-known superwind galaxy, NGC 1482 (see a review by Veilleux et al. 2005, for this and other examples). The non-uniform distribution of the density in the emission nebulosity is not surprising, because the optical emission lines are thought to originate from a boundary between hot bubble gas and cool ambient interstellar medium, fragmented under the action of Kelvin–Helmholtz and Rayleigh–Taylor instabilities.

Regions of modern star formation are located at the base of the wind and we have shown that ongoing star formation is concentrated almost entirely inside a ring less than 2 kpc in diameter. Gas is ionized not only by the radiation of OB stars, but also by shocks produced by the combined effect of supernovae and winds of massive stars, which transfer kinetic energy to the interstellar medium. The observed line-of-sight velocities in filaments are small and close to the systemic velocity, suggesting that these features consist of gas that was ejected from central regions and has preserved its angular momentum. The gas outflow occurs mostly in the sky plane and therefore the line-of-sight projection of the outflow velocity is small.

We adopt the characteristic length of the brightest filaments $l = 30$–35 arcsec (1.3–1.6 kpc) to derive the dynamic age of the emission feature $\tau_{\rm dyn} = l/v_{\rm out} \approx 10$–12 Myr. The total H$\alpha$ luminosity of the galaxy is $L_{\rm H\alpha} = 1.7 \times 10^{40}$ erg s^{-1} based on the observed

Hα+[N II] flux from Kaisin & Karachentsev (2008) and the average line ratio of log[N II]/H = −0.7. We assume that the wind radiation includes the flux from the regions located outside the ellipse with the semimajor axis 25 arcsec and axial ratio 0.4, which includes all H II regions in the disc. The wind luminosity is $L_{\rm H\alpha}$(wind) = 2.7 × 10^{39} erg s^{-1}. This makes up for 16 per cent of the total $L_{\rm H\alpha}$, and the south-east and north-west parts of the bipolar structure have almost equal luminosities (9 and 7 per cent, respectively). We now adopt, in accordance with Fig. 6, a mean electron density of $n_{\rm e}$ = 50 cm^{-3} to infer, in the same way as Matsubayashi et al. (2009), the total mass of ionized gas ejected from the disc,[2] $M_{\rm wind} = 1.7 \times 10^5$ $M_\odot$, and its kinetic energy $E = 5.8 \times 10^{52}$. We describe the emitting volume of the south-east part of the outflow wind by a truncated cone with the bases of diameters 30 and 40 arcsec to derive a characteristic filling factor for this volume $f \approx 3 \times 10^{-5}$. This value of f is indicative of the highly non-uniform nature of the emitting medium; Hα emitting gas is located mostly in the walls of the bubble, which fragment under the action of characteristic instabilities (Veilleux et al. 2005).

We now compare our inferred parameters with the wind parameters in two well-known nearby galaxies: M82 (Shopbell & Bland-Hawthorn 1998) and NGC 253 (Matsubayashi et al. 2009). The mass of the ejected gas in NGC 253 is almost the same as in our case, although the kinetic energy of the gas is twice as low and the formation time-scale of the feature is almost six times shorter. In M82, $M_{\rm wind}$ and E are greater by almost a factor of 30 and 360, respectively, with closer $\tau_{\rm dyn}$ = 3.4 Myr. The wind outflow velocities in these galaxies are three to four times higher than in NGC 4460. Given our remark about the uncertainty of measured $v_{\rm out}$, it can be concluded that, on the whole, the wind parameters in NGC 4460 are close to those observed in NGC 253, except for the fact that the emission nebulosity in NGC 4460 took much longer to form. This is not surprising, because the total star formation rate (SFR), formally inferred from $L_{\rm H\alpha}$, is almost 10 times higher in NGC 253. This fact most likely determines the relatively lower outflow velocity. In particular, we do not know whether the kinetic energy of the wind is sufficient for the gas to escape from the galaxy. A simple estimate of the escape velocity obtained in terms of the isothermal sphere model, with a cut-off radius of 2 arcmin, yields $v_{\rm esc} \geq 2.7 v_{\rm max} = 180$ km s^{-1} for regions located at galactocentric distances $r < 8$ arcsec, which is appreciably greater than $v_{\rm out}$. Therefore, most probably, after cooling down, the gas of the wind will fall back on to the galactic plane.

6.2 Cause of the burst of star formation

Thus, the central kiloparsec in NGC 4460 is engulfed in on-going star formation (SFR = 0.3 $M_\odot$ yr^{-1}; see Kaisin & Karachentsev 2008), in contrast to the old and 'quiet' disc of the galaxy. What could have triggered star formation in this lenticular galaxy? Tidal interaction with a companion is unlikely as the galaxy appears isolated. Nor is there any evidence for a merger of a gas-rich dwarf companion (the velocity field lacks kinematically decoupled components to be expected in such a case). No tidal features can be seen on optical images or published low-resolution H I maps (Sage & Welch 2006). The inner disc that we found in the brightness distribution proves that star formation has been going on for a long time in the centre; however, it is not indicative of interaction.

[2] In this analysis, we used information about the single phase of the wind, because Hα emission traces only the cooler interaction zone between the hot wind fluid and the ambient medium. Therefore, the values of $M_{\rm wind}$ and E are underestimated. However, we present these values for comparison with the similar values taken from similar analyses in other galaxies.

Table 2. Integrated parameters of isolated E/S0 galaxies within 10 Mpc.

	Parameter	NGC 4460	NGC 855	NGC 404
(1)	Type	SB(s)0+	E	SA(s)0-
(2)	Tidal index	−0.7	−0.8	−1.0
(3)	Distance (Mpc)	9.59	9.73	3.24
(4)	M_B (mag)	−17.89	−17.07	−16.61
(5)	M_K (mag)	−20.87	−20.15	−19.00
(6)	log M(H I) ($\odot$)	7.92	8.13	7.97
(7)	log [SFR] ($M_\odot$ yr^{-1})	−0.59	−1.07	−1.37
(8)	P_K^*	−0.11	−0.30	−0.14
(9)	F^*	−1.63	−0.94	−0.80

We have already pointed out above that isolated E and S0 galaxies are rare objects, and their integrated parameters differ appreciably from normal E and S0 galaxies in groups and clusters. Table 2 lists the basic parameters of all three representatives of this category of galaxies found within 10 Mpc from the Sun. Row 2 gives the tidal index according to Karachentsev et al. (2004); the distances in row 3 are from Tonry et al. (2001) for except NGC 404 (for which the mean value from Tonry et al. 2001 and Karachentsev et al. 2002 is accepted); rows 1, 4 and 5 give the observed parameters of the galaxies adopted from the NASA/IPAC Extragalactic Data base (NED); row 6 presents the H I mass from the HyperLEDA data base adopted for the accepted distances. Row 7 gives the estimated global SFR in galaxies inferred from their Hα fluxes from Kaisin & Karachentsev (2008) for NGC 4460 and from Karachentsev & Kaisin (2010) for the other two galaxies. Rows 8 and 9 give two dimensionless and distance-independent parameters (see Karachentsev & Kaisin 2007 and Kaisin & Karachentsev 2008 for details): $P_K^* = \log([\mathrm{SFR}] \times T_0/L_K)$ and $F^* = \log(M_{\rm HI}/[\mathrm{SFR}] \times T_0)$. The former characterizes the proportion of its luminosity the galaxy would produce during the Hubble time T_0 = 13.7 Gyr at the current rate of star formation and the mass-to-(K-band)-luminosity ratio $M/L_K = 1\,M_\odot/L_\odot$. The parameter F^* shows how much Hubble time the galaxy will need in future to use the present supply of gas if star formation proceeds at the currently observed rate.

Fig. 7 presents a distribution of 420 LV galaxies in the 'past–future' diagram (Karachentsev & Kaisin 2010). The isolated early-type galaxies of moderate luminosity that we have discussed are shown in red. Here, galaxies of different morphological types occupy essentially different regions in the diagnostic diagram. The median values of P_K^* and F^* for the total LV sample are −0.40 and −0.25, respectively. These quantities mean that a typical LV galaxy required a two to three times higher SFR in the past to reproduce its observed luminosity, also having enough gas to continue star formation with the observed rate for the next 8 Myr.

NGC 404, 855 and 4460 differ appreciably in luminosity, but have almost similar hydrogen masses: $\sim 1 \times 10^8$ $M_\odot$. The specific SFR per unit luminosity differs little among these galaxies. The parameter P_K^* is only slightly smaller than zero for all three galaxies. This indicates that the galaxies are capable of reproducing most of their stellar mass during cosmological time T_0, provided that star formation is at the current level. At the same time, the available gas reserves in these galaxies can maintain the current rate of star formation only for a short time-scale, ranging from 1/40 (NGC 4460) to 1/6 (NGC 404) of the age of the Universe.

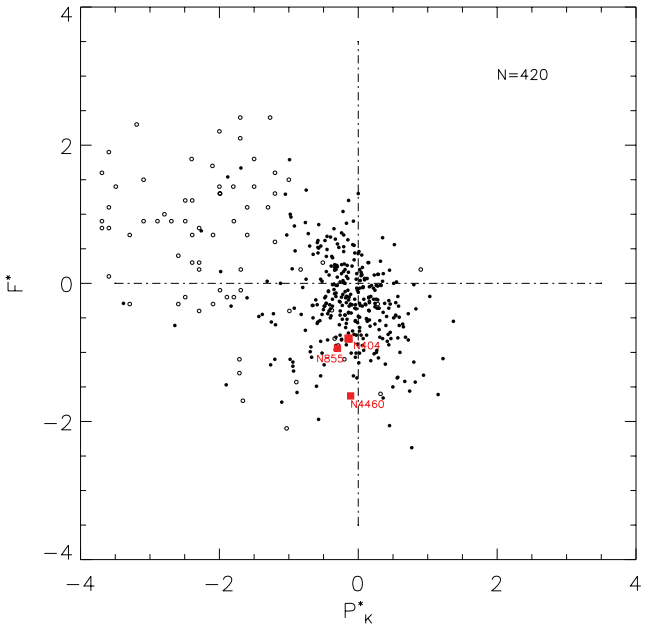

Figure 7. Evolutionary plane 'past–future' for 420 LV galaxies (Karachentsev & Kaisin 2010). The galaxies observed and detected in Hα are shown by filled symbols, and galaxies with only an upper limit of their Hα flux are indicated by open circles. The isolated E/S0 galaxies of moderate luminosity are distinguished by red squares and marked with their NGC numbers.

The location of isolated E and S0 galaxies on the diagnostic diagram $\{P_K^*, F^*\}$ does not allow us to view their observed evolutionary stage as a burst of star formation triggered by a merger of a companion or a single hydrogen cloud. Should this be the case, we would expect in the LV, in addition to the three isolated emission E and S0 galaxies mentioned above, an order of magnitude greater number of similar objects at the quiescent interburst stage. However, the currently available Hα-flux data for 420 galaxies of the LV (Karachentsev & Kaisin 2010) do not support the existence of such a population. Besides NGC 4460, 404 and 855, the LV contains only two other isolated galaxies: NGC 2787 (S0-a) and 4600 (S0), where very weak Hα emission is presented. These galaxies give blue absolute magnitudes of -18.5 and -15.7, respectively.

The predominance of objects with current central star formation among isolated E and S0 galaxies and their capability of reproducing the available stellar mass over the cosmological time-scale with the observed SFR combined with the scarcity of available gas reserves ($\sim 1 \times 10^8$ M$_\odot$) leads us to suggest that ongoing star formation in these galaxies is fed by an external source (i.e. intergalactic gas clouds or filaments). The process of external gas accretion should have a regular steady character on a cosmological time-scale, without significant bursts.

Recently, Kannappan et al. (2009) described a population of 'blue-sequence E/S0s' residing on the locus of late-type galaxies in colour versus stellar mass parameter space. They argue that these galaxies actively (re)grow their stellar discs and therefore may form a bridge between late-type spirals/iregulars and early-type red-sequence galaxies. Many low-to-intermediate mass blue-sequence E/S0s reside in low-density environments, and often have a blue centre and a substantial fraction of cold gas. However, their gas consumption time is usually smaller than 3 Gyr (Wei et al. 2010). All these properties are similar to those of the LV isolated E/S0 galaxies described above. Therefore, NGC 4460, 404 and 855 seem to belong to the population of blue-sequence E/S0s. Kannappan et al. (2009) suggest that these galactic populations connect with the disc rebuilding after major/minor merging or companion interactions. In this paper we have emphasized that accretion of external gas is also important in the particular case of evolution of isolated early-type galaxies.

7 SUMMARY

We have used available UV and optical images to explore the structure of the isolated lenticular galaxy, NGC 4460. We have also obtained long-slit and three-dimensional spectroscopic data in order to probe the origin of the bright Hα nebulosity surrounding the central region of the galaxy. We consider the following points to be most important.

(i) All ongoing star formation with a rate of about 0.3 M$_\odot$ yr^{-1} resides in a pseudo-ring with a radius of about 1 kpc. Together with the antitruncated shape of the surface brightness profile, this suggests the recent formation of the inner exponential disc, whose radial scale is three times smaller than the global old stellar disc.

(ii) Whereas gas in the circumnuclear disc is photoionized by radiation of young stars, the external regions of the Hα nebulosity are ionized by shocks. This fact, in combination with the bi-conical shape of the ionized gas nebulosity, with the radial distributions of the emission-line velocities and width, can be explained as a galactic-scale outflow (superwind) induced by central star formation. We have estimated the outflow velocity as $\geq$ 130 km s^{-1}. The galactic wind parameters, such as outflow velocity, formation time and total kinetic energy, are several times smaller compared with the known galactic wind in NGC 253, which is explained by substantially different SFRs.

(iii) We have also discussed the evolutionary status of NGC 4460, together with other isolated E/S0 galaxies in the LV: NGC 404 and 855. We have considered the position of the galaxies on the 'past–future' diagram (Karachentsev & Kaisin 2010). We have suggested that the continuous accretion of intergalactic gas is the most probable source of their current star formation. In contrast to the merging scenario, external gas accretion seems to be a sluggish process without violent events.

ACKNOWLEDGMENTS

The research is partly based on data obtained from the Multimission Archive at the Space Telescope Science Institute (STScI; MAST). The STScI is operated by the Association of Universities for Research in Astronomy, Inc., under the National Aeronautics and Space Administration (NASA) contract NAS5-26555. Support for MAST for non-*HST* data is provided by the NASA Office of Space Science via grant NAG5-7584 and by other grants and contracts. Funding for the SDSS and SDSS-II has been provided by the Alfred P. Sloan Foundation, the Participating Institutions, the National Science Foundation, the United States Department of Energy, NASA, the Japanese Monbukagakusho, the Max-Planck Society and the Higher Education Funding Council for England. The SDSS web site is http://www.sdss.org/. This research has made use of the NED, which is operated by the Jet Propulsion Laboratory, California Institute of Technology, under contract with NASA. We acknowledge the use of the HyperLeda data base (http://leda.univ-lyon1.fr). This work was supported by the Russian Foundation for Basic Research (project nos 09-02-00870, 07-02-00005 and 08-02-00627). AM is also grateful to the 'Dynasty' Fund. The authors thank the

anonymous referee for constructive advice that has helped us to improve the paper.

REFERENCES

Afanasiev V. L., Moiseev A. V., 2005, Astron. Lett., 31, 193
Afanasiev V. L., Dodonov S. N., Moiseev A. V., 2001, in Ossipkov L. P., Nikiforov I. I., eds, Stellar Dynamics: From Classic to Modern. Sobolev Astronomical Institute, St Petersburg, p. 103
Allen M. G., Groves B. A., Dopita M. A., Sutherland R. S., Kewley L. J., 2008, ApJS, 178, 20
Del Rio M. S., Brinks E., Cepa J., 2004, AJ, 128, 89
Erwin P., Beckman J. E., Pohlen M., 2005, ApJ, 626, L81
Heckman T. M., Dahlem M., Lehnert M. D., Fabbiano G., Gilmore D., Waller W. H., 1995, ApJ, 448, 98
Hubble E. P., 1926, ApJ, 64, 321
Kaisin S. S., Karachentsev I. D., 2008, A&A, 479, 603
Kannappan S J., Guie J. M., Baker A. J., 2009, AJ, 138, 579
Karachentsev I. D., Kaisin S. S., 2007, AJ, 133, 1883
Karachentsev I. D., Kaisin S. S., 2010, AJ, submitted
Karachentsev I. D. et al., 2002, A&A, 389, 812
Karachentsev I. D., Karachentseva V. E., Huchtmeier W. K., Makarov D. I., 2004, AJ, 127, 2031
Karachentsev I. D., Makarov D. I., Karachentseva V. E., Melnyk O. V., 2010, in Proc. Conf. Galaxies in Isolation: Exploring Nature vs. Nurture. Astron. Soc. Pac., San Francisco, arXiv:0907.4693
Kormendy J., Kennicutt R. C., 2004, ARA&A, 42, 603
Matsubayashi K., Sugai H., Hattori T., Kawai A., Ozaki S., Kosugi G., Ishigaki T., Shimono A., 2009, ApJ, 701, 1636
Moiseev A. V., Valdés J. R., Chavushyan V. H., 2004, A&A, 421, 433
Osterbrock D. E., 1989, Astrophysics of Gaseous Nebulae and Active Galactic Nuclei. University Science Books, Mill Valley, CA
Sage L. J., Welch G. A., 2006, ApJ, 644, 850
Shopbell P. L., Bland-Hawthorn J., 1998, ApJ, 493, 129
Stasińska G., Cid Fernandes R., Mateus A., Sodré L., Asari N. V., 2006, MNRAS, 371, 972
Thilker D. A., 2009, Galaxy Evolution Explorer, press release, http://www.galex.caltech.edu/newsroom/glx2008-02r.html
Tonry J. L., Dressler A., Blakeslee J. P., Ajhar E. A., Fletcher A. B., Luppino G. A., Metzger M. R., Moore C. B., 2001, ApJ, 546, 681
Veilleux S., Cecil G., Bland-Hawthorn J., 2005, ARA&A, 43, 769
Wei L. H., Kannappan S J., Vogel S. N., Baker A. J., 2010, ApJ, 708, 841
Westmoquette M. S., Gallagher J. S., Smith L. J., Trancho G., Bastian N., Konstantopoulos I. S., 2009, ApJ, 706, 1571

This paper has been typeset from a TEX/LATEX file prepared by the author.